REPORT DOCUMENTATION PAGE

Form Approved
OMB NO. 0704-0188

| 1. AGENCY USE ONLY (Leave Blank) | 2. REPORT DATE   02-28-07 | 3. REPORT TYPE AND DATES COVERED
Final Progress Report; 9/27/04 to 11/30/06 |
|---|---|---|

| 4. TITLE AND SUBTITLE
High Energy Density Nastic Structures Using Biological Transport Mechanisms | 5. FUNDING NUMBERS
W911NF-04-1-0421 |
|---|---|

| 6. AUTHOR(S)
Donald J. Leo	

| 7. PERFORMING ORGANIZATION NAME(S) AND ADDRESS(ES)
Virginia Polytechnic Institute and State University
301 Burruss Hall
Blacksburg, VA 24061-0249 | 8. PERFORMING ORGANIZATION
    REPORT NUMBER |
|---|---|

| 9. SPONSORING / MONITORING AGENCY NAME(S) AND ADDRESS(ES)
U. S. Army Research Office
P.O. Box 12211
Research Triangle Park, NC 27709-2211 | 10. SPONSORING / MONITORING
    AGENCY REPORT NUMBER
44287.1-MS-DRP |
|---|---|

11. SUPPLEMENTARY NOTES
    The views, opinions and/or findings contained in this report are those of the author(s) and should not be construed as an official Department of the Army position, policy or decision, unless so designated by other documentation.

| 12 a. DISTRIBUTION / AVAILABILITY STATEMENT
Approved for public release; distribution unlimited	12 b. DISTRIBUTION CODE

13. ABSTRACT (Maximum 200 words) A new mechanical actuation concept is demonstrated based on the controlled transport of fluid across semi-permeable membranes. This concept is based on the pressurization of cells similar to the process that plants use to maintain homeostasis and regulate cell function. In all plant systems, the transport of ions and fluid produce localized pressure changes (called turgor pressure) that perform many cell functions, such as maintaining cell integrity and controlling plant growth. In this article, we demonstrate that the concept of fluid transport caused by protein transporters can be used to control the actuation properties of a mesoscale device. The device considered in this work consists of two chambers separated by a semi-permeable membrane substrate that contains protein transporters suspended in a lipid bilayer. The protein transporters convert biochemical energy in the form of ATP into a protein gradient across the semi-permeable membrane. The proton gradient, in turn, induces a flow of fluid across the porous substrate and pressurizes a closed volume. The experimental demonstration uses a directly applied gradient. The pressurization of the closed volume produces a deformation in the cover plate of the chamber, thus transforming the chemical energy of the ATP into a measurable motion in the actuator. Experiments on the device demonstrate that micron-scale displacements can be induced in a millimeter-scale actuator. The time constant of the response is on the order of tens of seconds, and results demonstrate that the pH gradient (or) amount of ATP and ATPase control the actuation properties of the device. To our knowledge, this is the first demonstration of using natural protein transporters as the active component of a mechanical actuator.

| 14. SUBJECT TERMS
nastic structures, microhydraulic actuator, bio-inspired actuation, biological protein channels, chemomechanical actuation | 15. NUMBER OF PAGES
33 |
|---|---|
| | 16. PRICE CODE |

| 17. SECURITY CLASSIFICATION
OR REPORT
UNCLASSIFIED | 18. SECURITY CLASSIFICATION
ON THIS PAGE
UNCLASSIFIED | 19. SECURITY CLASSIFICATION
OF ABSTRACT
UNCLASSIFIED | 20. LIMITATION OF ABSTRACT
UL |
|---|---|---|---|

NSN 7540-01-280-5500

Standard Form 298 (Rev.2-89)
Prescribed by ANSI Std. 239-18
298-102

Contents

List of Figures

List of Tables

1   Statement of the problem studied

The focus of this research effort was to develop a new class of structural materials that incorporate engineered biological transport mechanisms for the development of high-energy density actuators. The goal of the Phase I effort was to demonstrate the synthesis, design, and fabrication of a device that exhibits controllable actuation using biological transport mechanisms.

2 Summary of the most important results

2.1 Biological Transport through Proteins in Reconstituted Membranes

The development of actuators and actuation mechanisms over the last fifty years were based on electro-mechanical coupling observed in a variety of engineering materials. The conversion of readily available electrical energy accelerated the acceptance of these materials into engineering devices. Plants and animals are energy conversion systems that convert naturally available forms of energy into other forms that can be readily used in cells. The energy available in biological fuels like Adenosine triphosphate, kinesin etc., are comparable to that of popular hydrocarbon fuels. The ATP synthesized in plant cells is the energy source for translation and a variety of life functions. Translation in plants occurs due to fluid transport through protein transporters embedded in cell membranes. Our idea is to develop a hybrid actuator combining the active components protein transporters extracted from plant cells with synthetic polymers. The microhydraulic actuation mechanism is inspired by the ion transport process across cell membranes.

2.1.1 Ion Transport in Plant Cells

Transport of ions in plants can be classified into three major types: Active transport, secondary active transport and osmotic regulation[1]. Active transport initiates transport in cells by moving ions through protein pumps expending chemical energy. The transmembrane potential across the cell membrane resulting from active transport opens ion channels that conduct ions and solutes to maintain electroneutrality. The transport of species through ion channels from the established electrical or ionic gradient is called secondary active transport. The active and secondary active processes occur at the cell wall and membranes of inter-cellular organelles to transport nutrients in the plant. The concentration of ions from the active and secondary active transport processes increases the osmolarity inside the cell. This results in water to permeate through the cell membranes into the cytoplasm and cause volumetric expansion. In certain plants like the bladderwort and Venus flytrap the leaves snap close in 150 ms to catch its prey[2]. The rapid response to snap the leaves close results from sudden loss in turgor pressure established by ion transport[3, 1]. All the biological processes observed in the plants use chemical energy from bio-fuels to maintain life and increase in volume and to demonstrate observable mechanical actuation.

The ion and fluid transport processes inherent in plants serves as the template for the bio-inspired actuation mechanism discussed in this article. The actuator device - referred to as a microhydraulic actuator - uses ion transporters extracted from plants that move ions and fluid to generate force. In this work we utilize a protein pump that is responsible for the movement of sugars, ions, and fluid within certain types of plants. There are different types of sugars synthesized in plants and plant cells have evolved to transport them through the cell membranes to maintain life[4]. Sucrose moves through the cell membrane together with a proton or is exchanged for a proton at the cell membrane through protein pumps/channels. Depending on the direction of proton-sucrose movement, the transport of proton-sucrose in plants is classified into two types - cotransport and antiport [5, 6]. A proton-sucrose cotransporter SUT4,

ACTUATION IN PLANT CELLS

ATP Hydrolysis

Ion Transport processes

Osmotic regulation

Concept observed in plants for deformation and growth

ACTUATION CONCEPT BASED ON BIOLOGICAL ION TRANSPORT

Strong synthetic shells – mimic transport properties of cell membranes

Actuator – capability to change shape due to ion movement

Relative expansion and contraction of alternative layers of synthetic shells

Figure 1: Actuation concept: Using fluid transport in plant cell membranes for actuation

commonly found in Arabidopsis thaliana and other higher plants was identified and reported by Frommer et. al[7]. Further investigation by Frommer's group following their first report in 2000 characterized the transporter protein[8, 9, 10]. The SUT4 transporter protein is reported to be selectively permeable to proton, sucrose and water molecules[7]. The transporter conducts proton, sucrose and water down a concentration gradient of sucrose in the presence of a favorable proton motive force. This selective nature of the transporter is favorable for hydraulic actuation, as the proton gradient will provide the required proton motive force for transport and concentration of sucrose will serve as the control parameter.

In addition to proton gradient driven transport, the SUT4 transporter protein can be used for fluid transport powered by the biochemical reaction starting from Adenosine triphosphate (ATP). In the presence of ATP and Adenosine triphosphatase (ATPase) enzyme, the protein transporter has the ability to move a proton, sucrose and water without an applied proton
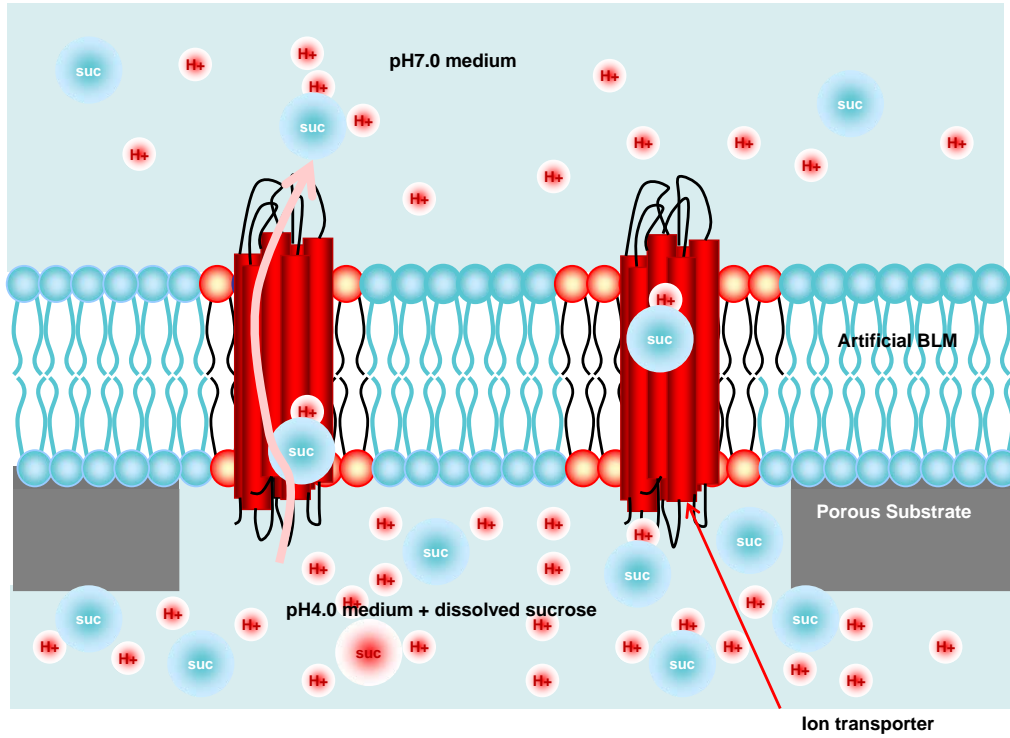
Figure 2: Schematic of the Membrane Assembly - Ion transporter reconstituted in artificial bilayer lipid membrane supported on porous substrate

gradient[11]. For this reason it is possible to use ATP to control the flow of fluid through the protein pumps for the purpose of creating a mechanical actuator. These molecular machines can transport fluid only when formed in a membrane very similar to the cell membrane[12]. The transporter proteins must be suspended in a supporting membrane to function properly. Generally the protein transporters are suspended in a bilayer lipid membrane (BLM) self-assembled from a phospholipid mixture. The bilayer lipid membranes (BLM) formed from phospholipid molecules are very similar to cell membranes and can accommodate the transporter protein on porous solid supports [13]. The BLM serves as the host membrane for the transporter proteins and is shown schematically in Figure 2. The BLM with the ion transporter supported on a solid porous substrate forms the active part of the actuator. The membrane assembly with the transporter proteins is subjected to the concentration gradient that will result in fluid transport through the membrane.

2.1.2 Prototype Actuator Device

The first generation prototype actuator is built around the membrane assembly shown in Figure 2. The actuator has a cover plate with cavities that form the barrel, the membrane assembly and a fluid reservoir. The membrane assembly forms the controlled pathway for fluid transport from the fluid reservoir into the barrel as shown in Figure 3. The fluid reservoir contains the

pH4.0 buffer with sucrose and the barrel contains pH7.0 buffer. The solutes in the chamber on the either sides of the membrane assembly provide the chemical stimulus for fluid transport into the barrel. A deformable membrane seals the barrel from top and any additional fluid in the barrel from transport results in an increase in fluid pressure and deforms the membrane. The deformation of the membrane in an array of barrels increases the effective thickness of the actuator and can be considered as strain in the thickness direction of the actuator. The deformation experiments presented in this article are restricted to a single barrel device called the prototype actuator device. The experiments on the prototype actuator will validate the concept and provide us with an estimate of the concentrations for the chemical stimulus that will cause an effective increase in thickness in the actuator.

$$F = -K\Delta x$$

$$F = -\Delta P A$$

$$\Delta V = A\Delta x$$

$$\Delta V$$

- Deformable membrane
- Barrel
- Membrane assembly
- Fluid reservoir
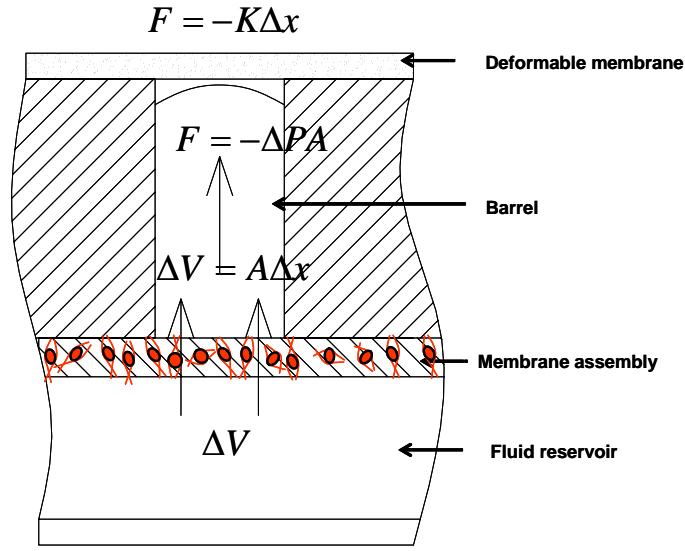
Figure 3: Fluid transport in a single microhydraulic actuator plate to result in deforming the coverplate of the actuator

2.1.3   Materials and Experimental Methods

The SUT4 cotransporter proteins are supplied to us from the University of Cincinnati. The SUT4 gene extracted from Arabidopsis thaliana was expressed in yeast cells and produced in large quantities. The SUT4 ion transporters, cultured in yeast cells were extracted, purified and stored as a suspension in pH7.0 medium. The lipids forming the BLM - 1-Palmitoyl- 2- Oleoyl- sn- Glycero-3-Phospho- L-Serine (Sodium Salt) (POPS) and 1- Palmitoyl- 2-Oleoyl- sn-Glycero-3-Phosphoethanolamine (POPE) are supplied by Avanti Lipids Inc., Alabaster, AL, USA. The photocurable poly-propylene glycol barrel (ϕ8mm x 4 mm) and the reservoir (ϕ8mm x 4 mm) were provided by SRI International, Palo Alto, CA, USA. The track etched polycarbonate membrane discs with the 1.2 μm pores were supplied by Millipore, Billerica, MA, USA. The Mylar

8

membrane was purchased from Scientific Precision Instruments.

2.1.4 Proton Gradient Driven Transport

The membrane assembly in the microhydraulic actuator is the active component that conducts fluid. The experiment focuses on demonstrating active transport across an artificial BLM with reconstituted ion transporters. The artificial BLM is supported on a porous Lead silicate glass plate at the base of a transport assay cup and quantify the flux. The experiment can be divided into the following three steps:

1. Forming the BLM

2. Reconstituting ion transporters in the BLM to render it functional

3. Demonstrating controlled transport through the functional BLM
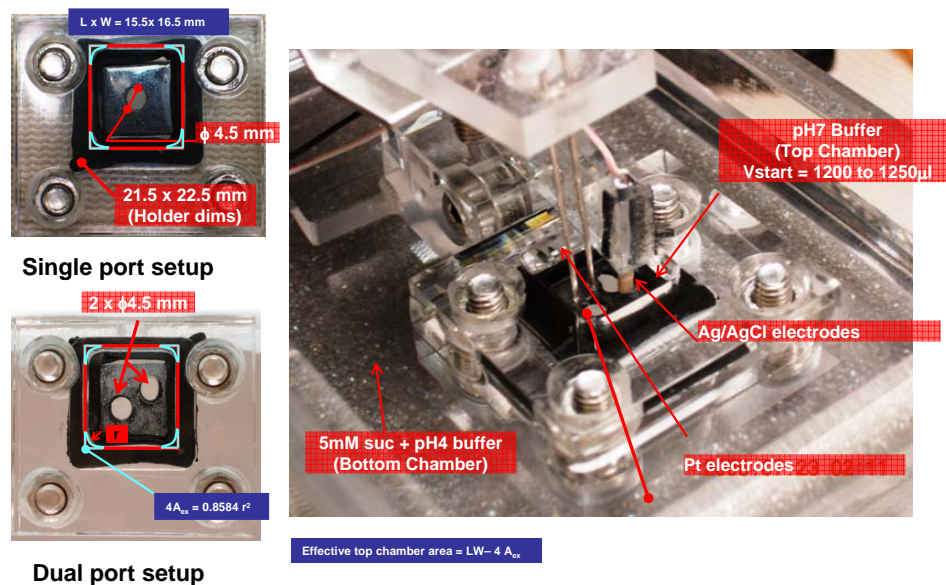
Figure 4: Experimental Setup for fluid transport through glass plates supporting the membrane assembly

The SUT4 transporter protein was reconstituted in POPS:POPE BLM supported on a porous lead silicate glass plate with 50 μm pores. The formation of a BLM across the pores was verified by impedance measurements reported in Sundaresan et. Al [14]. The glass plate was clamped in a fixture and introduced in reservoir that provided the required pH and sucrose gradient. The pH gradient was kept a constant at 1000 fold and sucrose concentration was varied to characterize the fluid flux for different sucrose concentrations (1 mM, 5 mM, 10 mM, 20 mM) in the reservoir. A flux rate of 1.58 μl/ cm2-μg(SUT4)-min was measured through the membrane for pH4.0+10mM sucrose/pH7.0 gradient applied across the membrane. Flux rates extracted from this data and plotted against the concentration of sucrose demonstrate that there is an

increase in flux as the concentration of sucrose increases in the pH4.0 medium as shown in Figure 5 (b). These results demonstrated the feasibility of transporting fluid through the lipid membrane with ion transporters and demonstrated the dependence of sucrose concentration on the flux rate.
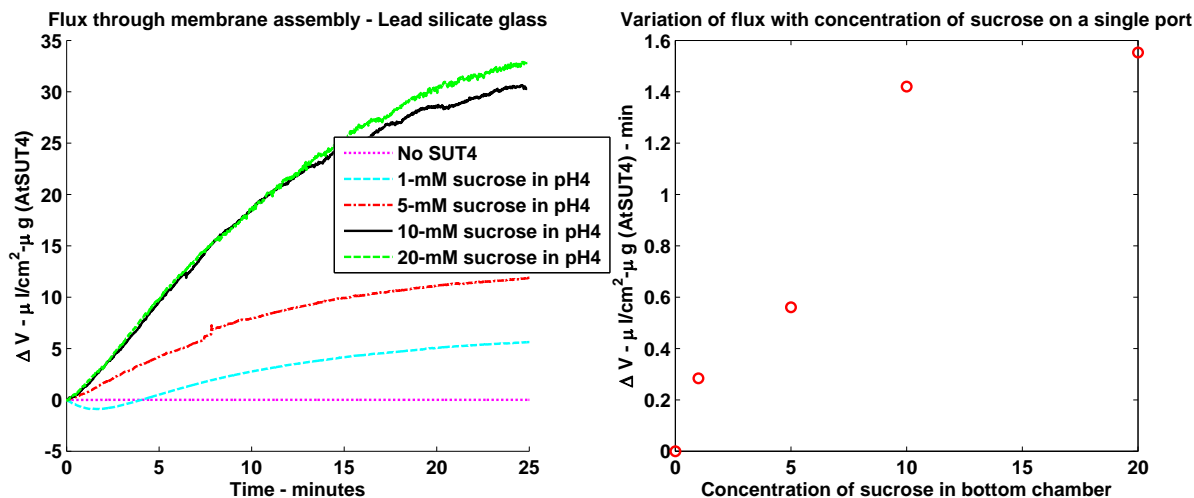
Figure 5: Measured fluid flux through the membrane assembly supported on lead silicate glass plate

2.1.5 ATP-powered Transport

The SUT4 transporter is reported to actively transport sucrose expending ATP by Truernit et. al [11]. We attempted to leverage this idea for actuation and quantified the fluid flux through the transporter due to ATP hydrolysis in the protein. The biochemical reaction is an ATPase enzyme catalyzed reaction. The schematic described in Figure 6 shows the mechanism by which ATP hydrolysis establishes a pH gradient locally across the transporter to transport sucrose. ATP fuel was added to the top chamber as Mg-ATP salt dissolved in pH7.0 buffer. The SUT4 transporters are added onto the porous lead silicate glass plates with the ATPase enzyme. The SUT4 proteins are available as vesicles with the yeast cell membranes. They spread on the lipids added to the substrates and form into a planar BLM, inserting the protein across the membrane as shown in the schematic in Figure 6. The enzyme helps to bind the ATP molecule to the protein and establishes a localized proton gradient across the transporter. This serves as a trigger for proton and sucrose transport through the membrane. The sucrose transported through the protein also carries water molecules with it to result in bulk fluid transport.

The red beet ATPase added to the BLM was varied to study the effect of the quantity of the enzyme that catalyzes the reaction and hence fluid transport. The BLM was formed with pH7.0 buffer carrying 10 mM sucrose supporting it at the bottom and pH7.0 buffer with Mg-ATP salt in the top and dispersed with SUT4 transporters. As a control study, enzyme was not added to the lipids and the flux was recorded for 10mM sucrose and 5mM ATP in the bottom
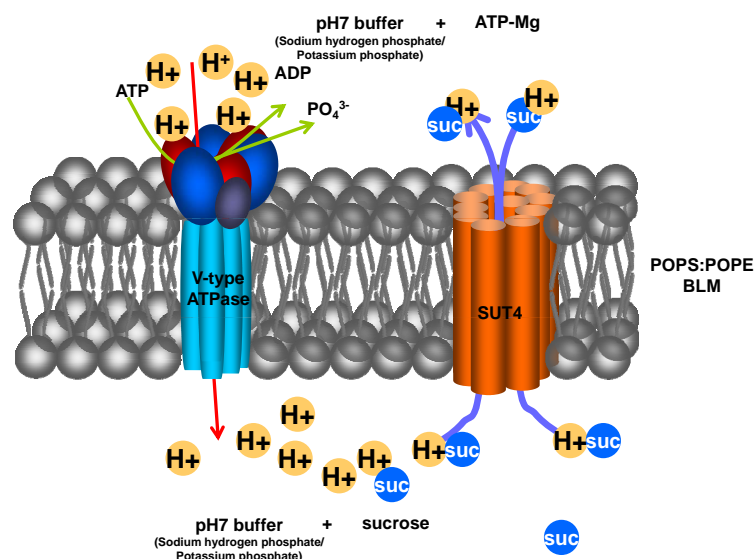
Figure 6: Schematic of fluid transport through the membrane assembly resulting from ATP hydrolysis in the transporter

chamber and top chamber respectively. In the absence of ATPase enzyme, hydrolysis of ATP is not initiated and hence no transport was observed. In the next trial, enzyme was added to the BLM. Plain pH7.0 buffer without ATP fuel was added to the top chamber. Along expected lines, no transport of fluid was observed due to the absence of ATP. In subsequent trials, the amount of the enzyme added to the plates was varied. Results in Figure 8 shows a representative data for the total flux observed for 3 μl, 6 μl and 12 μl of enzyme added to the bilayer. The plots (a), (b) and (c) in Figure 7 shows the change in volume with time in top chamber normalized with respect to the area of the BLM and amount of SUT4 transporters for different amounts of ATPase enzyme. The plot in Figure 7 shows the normalized flux rate for different amounts of enzyme added to the BLM with 95% confidence interval obtained from t-distribution (8 trials at 3 μl, 6 μl and 3 trials at 12 μl of enzyme). It is observed from this plot that ATP in the presence of ATPase enzyme results in fluid flux against gravity into the top chamber. Flux rate is observed to be dependent on the amount of enzyme added to the BLM. The flux peaks in the first 5 minutes of the experiment for 6 μl of ATPase enzyme in the BLM and in the first minute for 12 μl enzyme added to the BLM. The flux rate decreases after the initial spike and settles at a steady value for the next 15 minutes under observation as shown in plots (a), (b), (c) in Figure 7. The initial rate (flux through transporter for the first minute) observed for ATP powered transport in Figure 7 is plotted from individual results shown in Figure 8. The initial rate for the ATP powered transport is approximately 8-10 times higher than the rate observed with proton concentration gradient driven transport shown in plot (b) in Figure 5.

The negative flux observed in Plot(a),(b), (c) in Figure 7 are in the absence of the ATPase reaction in the medium. In the absence of the biochemical reaction, the experimental results indicate the flow of fluid from the top chamber to the bottom chamber. This is due to osmotic regulation resulting from higher concentration of sucrose in the bottom chamber. Since water

11
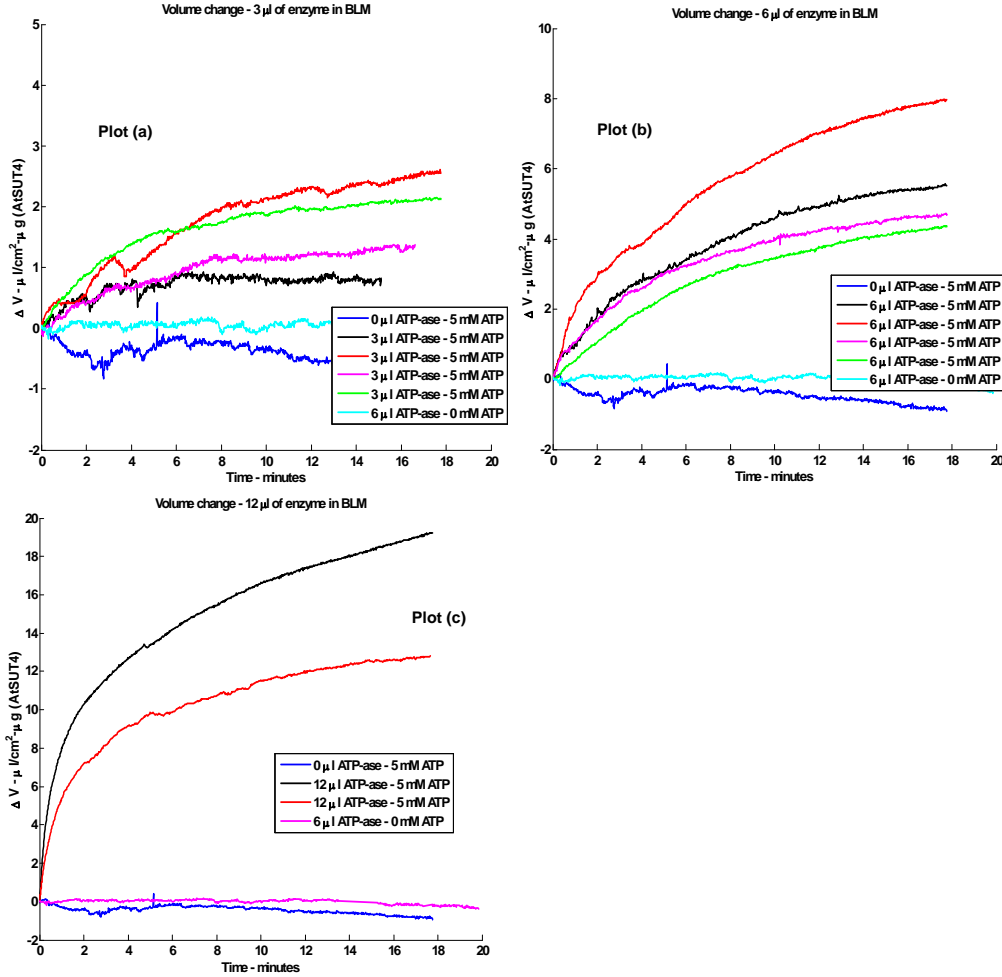
Figure 7: Measured fluid transport through the membrane assembly for different amounts of catalyzing ATPase enzyme reconstituted with SUT4

molecules are permeable through the BLM, the top chamber drains to maintain osmolarity.

2.1.6 Experimental Demonstration of Actuation

A schematic of the actuator is shown in Figure 10 alongside with the fabricated components for the prototype. The barrel (ϕ 8mm x 4 mm) and the fluid reservoir (ϕ 8mm x 4 mm) are fabricated from photocurable poly-propylene glycol diachrylate (PPG-DA). The track etched polycarbonate membrane discs with pores (1.2 μm) serve as the porous substrate and is attached to the barrel as shown in Figure 10. Tubes are attached from the fluid reservoir to the feed reservoir to provide a constant supply of sucrose and pH4.0 buffer. A Mylar membrane measuring 2.5 μm in thickness supported on transparent tape forms the deformable membrane of the actuator element. The POPS and POPE are mixed in the ratio 3:1 in n-decane (40 mg/ml) and spread

Flux rate as a function of the amount of enzyme added to the BLM
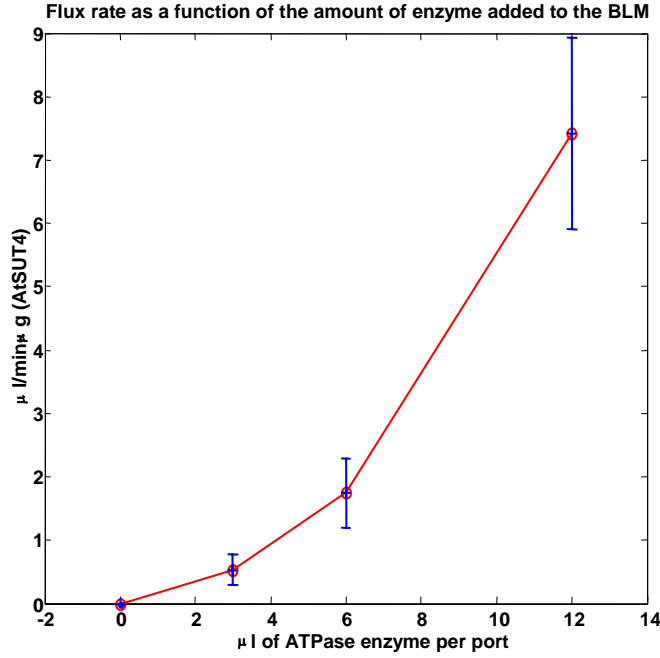
Figure 8: Measured fluid flux normalized with respect to membrane area, amount of transporters-SUT4 vs. amounts of enzyme in the membrane assembly

on the polycarbonate membrane. The SUT4 transporter suspension is added above the lipids and allowed to stand for 15 minutes. The barrel is assembled with the reservoir and pH7.0 buffer is added to it. The mylar membrane with a deformable diameter of 4.5 mm is clamped above the barrel in the fixture to result in the assembled configuration shown in Figure 9. The total thickness of the assembled actuator is 8 mm. The data acquisition system for measuring the deformation in the mylar membrane of the the microhydraulic actuator is shown with the assembled actuator in Figure 9. A polytec laser vibrometer is used to measure the deflection of the reflective spot at the center of the mylar membrane. The vibrometer head is connected to a Windows 2000 workstation through the vibrometer controller and dSpace data acquisition board (DS1104). Displacement and velocity are recorded using 2 of the 8 channels available in the dSpace RTI 1104 DAQ board with Matlab R12 and Control Desk 2.1. The assembled actuator is placed on a granite table to prevent structural vibration from being passed onto the fixture while measuring the deformation using the laser vibrometer. The concentration gradient of sucrose from the fluid reservoir in the presence of a pH gradient forms the input to the microhydraulic actuator element. The pH gradient across the membrane is maintained at 1000 (pH4.0 - in the fluid reservoir and pH7.0 in the barrel). The concentration of sucrose in reservoir is varied in the fluid reservoir to control the fluid flux into the barrel and hence the deformation in the Mylar membrane. The different trials performed on the actuator are:

1. No sucrose in the fluid reservoir

2. 10 mM sucrose in the fluid reservoir without SUT4 in the BLM
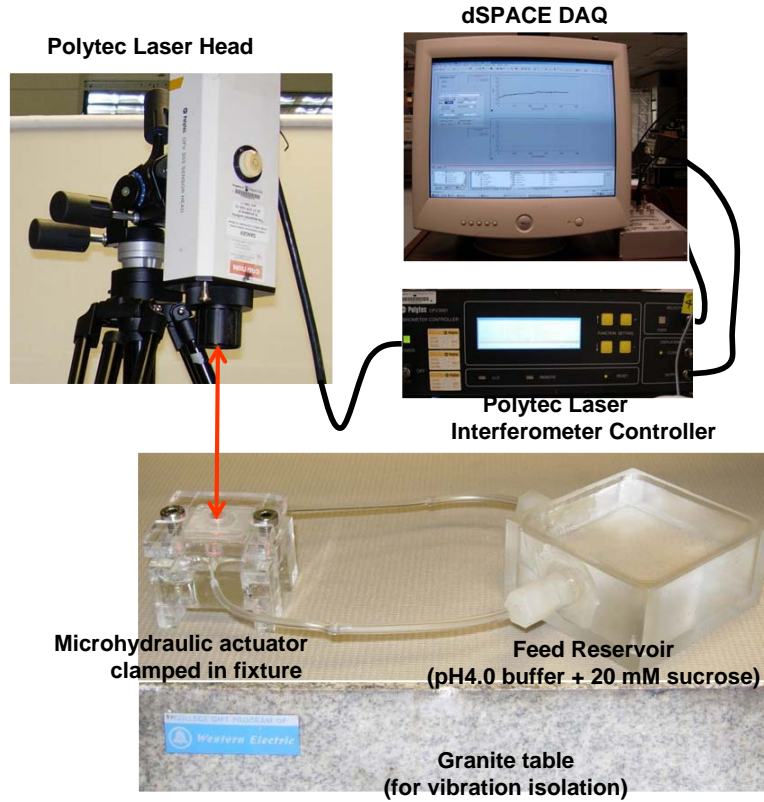
Figure 9: Experimental setup to measure deformation in prototype actuator

3. Various concentrations of sucrose in the fluid reservoir - 5 mM, 20 mM and 30 mM

The results for the different test cases are available in Figures 11 and 12. We were able to repeat 5 working trials for each test case and the plots show representative samples for the respective cases. The plot (a) in Figure 11 shows the recorded deformation for different baseline measurements. It is observed that in the absence of sucrose in the reservoir, there is no deformation in the Mylar membrane. This confirms the selectivity of SUT4 transporter protein as discussed by Weise et. al[7], Kuhn et. al[9] and reported in our earlier findings[15, 16]. The same plot shows that the Mylar membrane concaves when there is no SUT4 transporter protein in the BLM. We think this is due to the permeability of BLM to water molecules. In the absence of transporter proteins and 10 mM sucrose in the reservoir, there is an osmotic gradient from the barrel to the reservoir. This results in water molecules from the barrel diffusing through the BLM to the reservoir side to maintain osmolarity. This decreases the pressure in the barrel and causes the Mylar membrane to deform into the barrel. This also demonstrates the impermeability of the BLM to sucrose molecules. The measured results also clearly demonstrate that deformation is a function of the sucrose concentration in the actuator. The deformation observed in the Mylar membrane saturates at a mean value of 8.25 μm for 5mM sucrose and at 29.64 μm for 20 mM sucrose in the reservoir for 8 trials performed at each concentration. At higher sucrose concen-

14
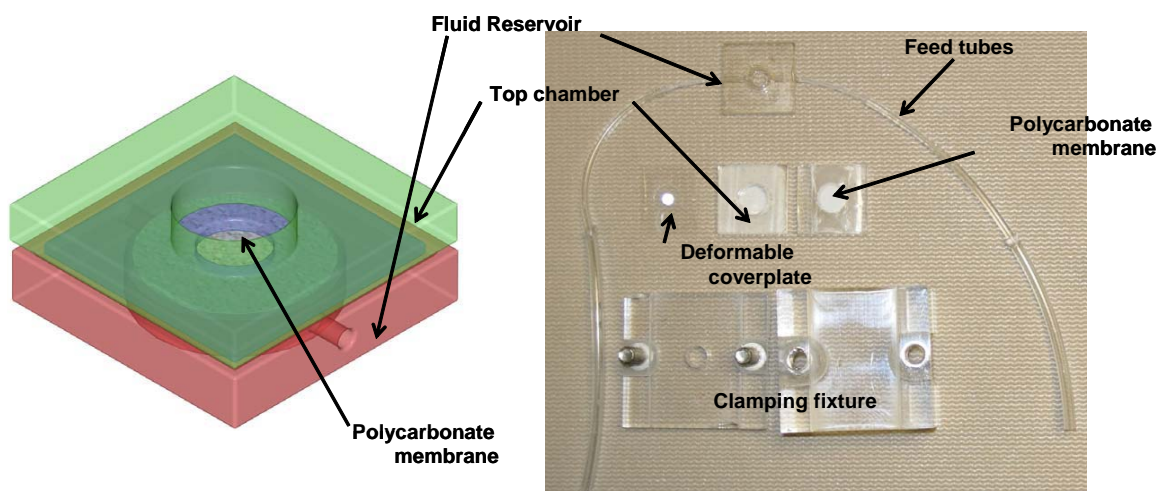
Figure 10: Microhydraulic actuator element - Schematic and fabricated prototype

trations, the deflection is observed to be smaller than that for 20 mM sucrose. We attribute the smaller deformation in the Mylar membrane at higher concentrations of sucrose to the back flow of water from the barrel to the fluid reservoir due to the huge osmotic gradient. At higher sucrose concentration in the bottom chamber, we predict that the osmotic gradient decreases the net effective flux through the membrane and hence the deformation.

2.2 Mechanical Characterization of Lipid Membranes

In order to successfully integrate a BLM into an engineering application it is necessary to quantify the mechanical properties of the membrane. Investigators in biomechanics have long been interested in studying the mechanical behavior of spherical shells of lipid bilayers, known as vesicles, because they resemble the spherical shape of cell membranes. The micropipet aspiration technique that was pioneered by Mitchison and Swann [17] and has been developed extensively by Evans and Needham [18] is among the best established methods for measuring the mechanical properties of vesicles. Several other methods have also been adopted to test BLMs such as atomic force microscopy, magnetic twisting cytometry, and cytoindentation [19].

The purpose of this work was to measure the maximum pressure that a lipid bilayer can withstand when it is formed over a rigid substrate containing an array of circular pores. Using a porous substrate as a support structure for the formation of a BLM has been used as a technique to enhance its stability [20, 21]. In a previous study, a custom test fixture was developed to measure the failure pressure of a BLM formed on a porous substrate [22]. In this procedure, a porous polycarbonate substrate was coated with a BLM and then clamped between the bottom piece and the base of the test fixture shown in Figure 13. The lipid bilayer was submerged in an aqueous salt solution and then additional salt solution was steadily poured into the upright cylindrical tube positioned above the BLM, which increased the hydrostatic pressure applied to

15
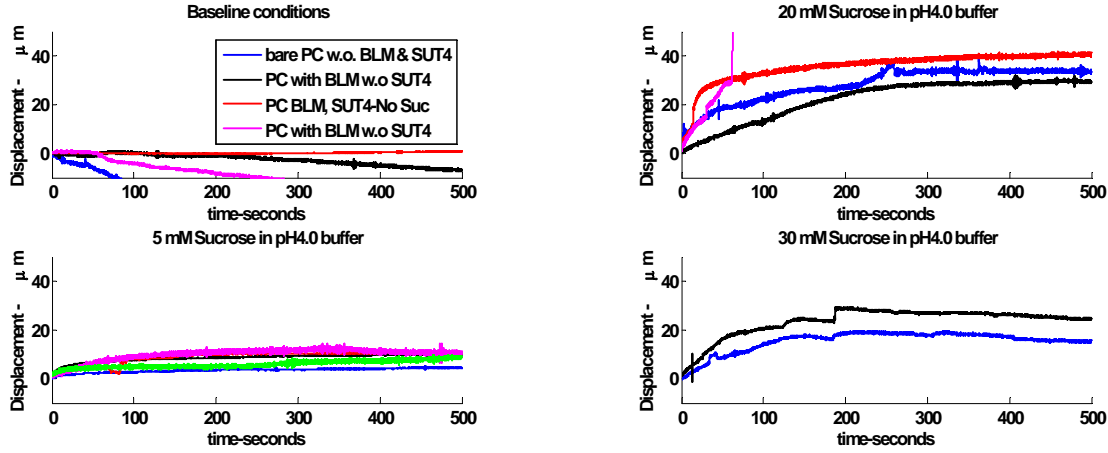
Figure 11: Measured deformation in actuator for pH gradients - baseline and 5 mM sucrose

Figure 12: Measured deformation in actuator for pH gradients - 10 and 20 mM sucrose

the lipid bilayer. The lipid bilayer was capable of supporting the water column until a critical pressure was reached, at which point the height of the water column was observed to drop. This critical pressure will be referred to as the failure pressure of the BLM.

Several types of lipids were tested including 1-Stearoyl-2-Oleoyl-*sn*-Glycero-3-Phosphocholine (SOPC) and mixtures of SOPC and cholesterol (CHOL). Mixtures of SOPC/CHOL were used because studies have shown that cholesterol increases the strength of BLMs [23, 24]. They have further concluded that cholesterol concentrations of $50 - 60$ mol% will maximize the strength of an SOPC/CHOL BLM, which was the basis for the concentration chosen for this study. This test was repeated for different substrate pore radii to produce a plot of the mean failure pressure versus substrate pore radius. The previous results from the water column test fixture are reviewed later in this paper. A trend of increasing failure pressure with decreasing pore size was observed.

The data measured in the previous study was limited to small pressures and therefore substrates with relatively large pore sizes. In an effort to increase the range of pore sizes that could be tested, while also increasing the accuracy and precision of the experiments, a new experimental test fixture was developed. In this test fixture, a stepper motor is used to drive a piston attached to a lead screw. The stepper motor applies pressure in very fine increments (approximately 300 Pa/step but varying with the pressure range) to the internal lower chamber of the test fixture that is sealed with a BLM formed on a porous substrate. The resulting pressure curve is monitored using a pressure transducer, and the maximum pressure achieved before failure of the BLM is recorded as the failure pressure. As with the previous study, this test was performed using various pore sizes to produce a plot of the mean BLM failure pressure versus substrate pore radius.

Finally, the characteristic pressurization curve of a BLM was modeled according to the pressurization and flow of fluid through the porous substrate. Initially pressure increases as the moving piston creates a load on the fluid in a closed system. Upon reaching the failure pres-

16
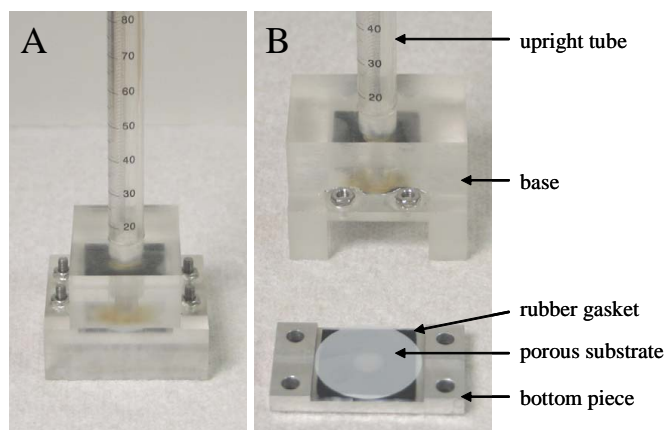
Figure 13: Photograph of the water column test fixture, (A) assembled, and (B) disassembled.

sure of the BLM, pressure decreases as fluid escapes through the porous medium. Since the BLM is formed over many pores, the setup can be thought of as an array of micro-BLMs covering the many pores. Every BLM does not fail at precisely the same pressure, but rather the failure pressure follows a statistical distribution, which in this case was assumed to be a normal distribution.

2.2.1 Materials and Methods

SOPC and cholesterol were purchased in powder form from Avanti Polar Lipids (Alabaster, AL). The lipid powders were dissolved in n-decane (99% purity, Alfa Aesar, Ward Hill, MA) at a concentration of 40 mg/mL and mixed for 30 minutes using a sonicator (model 50, VWR, West Chester, PA). For some experiments SOPC was mixed with cholesterol to create stronger BLMs. In particular, 50 mol% cholesterol was added to SOPC. The BLMs were reconstituted in an aqueous salt solution over Isopore polycarbonate membrane filters acquired from Millipore (Bedford, MA). The aqueous salt solution was prepared with 0.1 M NaCl (100.0% purity, Mallinckrodt Baker, Inc., Paris, KY) and deionized water. The porous polycarbonate substrates were treated by the manufacturer with a hydrophilic polyvinylpyrolidone coating which facilitates the formation of a BLM on its surface. Tests were performed for pore diameters of 0.05 μm, 0.1 μm, 0.2 μm, 0.4 μm, 0.8 μm, 2 μm, 5 μm, and 10 μm. For modeling purposes it was also necessary to know the thickness, which was provided by the manufacturer, and the permeability, which was determined experimentally. These values are reported in Table 1. Measuring permeability is further explained in Section 2.2.3.

Experiments were carried out to evaluate the failure pressure of planar BLMs. The test fixture for this study was composed of a stepper motor (model L1MGJ-M200XX060, EAD Motors, Dover, NH) used to drive a lead screw in a linear motion. A piston with an outside diameter of 12.2 mm was attached to the end of the lead screw, which had a thread pitch of 1.57 threads/mm. For each step the motor turns $0.9°$, which translates into a linear piston motion of 1.59 μm. The piston was used to pressurize a lower fluid chamber inside of the aluminum

17

Table 1: Specifications for porous polycarbonate substrates.

Pore Dia. (μm)	Thickness (μm)	Permeability (m^2)
0.05	10	2.5 x 10^{-18}
0.1	10	2.0 x 10^{-17}
0.2	10	8.0 x 10^{-17}
0.4	10	2.0 x 10^{-16}
0.8	9	1.9 x 10^{-16}
2	8	3.0 x 10^{-16}
5	15	4.2 x 10^{-15}
10	10	1.2 x 10^{-14}

Figure 14: Schematic of the stepper motor test fixture.

body of the test fixture, which had an internal volume of 5.0 mL (see Figures 14 and 15). The lower fluid chamber in the aluminum body was connected to a polycarbonate upper chamber via a 3.2 mm diameter hole. The lower and upper chambers were sealed using rubber gaskets. The porous substrate was clamped between the lower and upper fluid chambers so that the lower fluid chamber was under pressure and the upper chamber was open to the atmosphere. A pressure relief valve was connected to the lower fluid chamber and a polycarbonate fluid reservoir. The pressure relief valve remained open while the porous substrate was clamped into place and was then closed before the test was started. This procedure was necessary to prevent an initial pressure buildup during assembly.

Pressure was monitored by two different pressure transducers that had different ranges. A pressure transducer with a range of $0 - 690$ kPa (model PX181B-100G5V, Omega Engineering, Inc., Stamford, CT) was used for pore sizes from $0.05 - 0.2\,\mu$m and a pressure transducer with a range of $0 - 41$ kPa (model PX181B-006G5V, Omega Engineering, Inc., Stamford, CT) was used for pore sizes from $0.4 - 10\,\mu$m. Both pressure transducers are reported by the manufacturer to have an accuracy of 0.3% of full scale. Pressure was recorded using a multifunction data acquisition module (model USB-6009, National Instruments, Austin, TX) and Labview software (National Instruments, Austin, TX).

For each experiment a porous substrate was coated with 20 μL of lipid/n-decane mixture by

Figure 15: Photograph of the stepper motor test fixture, (A) assembled, and (B) disassembled.

using a pipettor (model Calibra 822, Socorex, Switzerland) and was then clamped between the lower and upper fluid chambers. Pressure was slowly applied by running the stepper motor at a fixed frequency of 1 Hz for the entire duration of the test. The failure pressure of the BLM was determined at the point when pressure began to decrease in the lower chamber of the test fixture. Ten trials were performed for each combination of lipid mixture and substrate pore size. Control 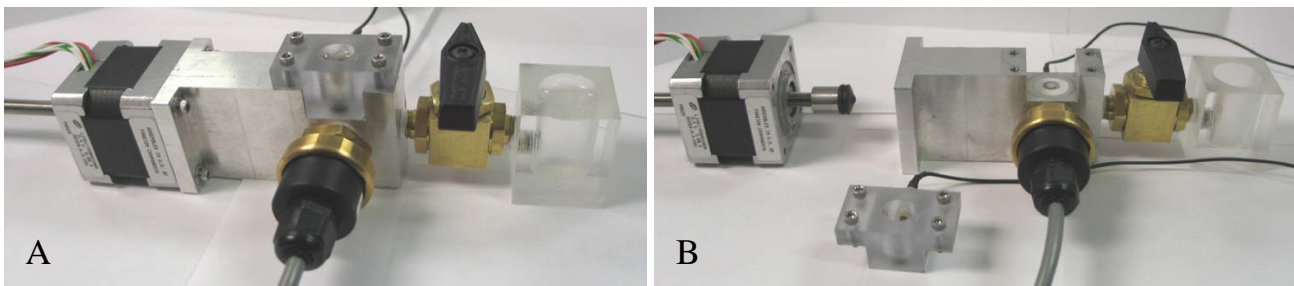trials were also performed for each pore size. For control trials a porous substrate with no BLM was clamped into the stepper motor test fixture. The stepper motor was run at a frequency of 1 Hz and pressure was recorded.

A silver/silver-chloride (Ag/AgCl) electrode (model EP2, World Precision Instruments, Inc., Sarasota, FL) was mounted on either side of the porous substrate so that it was submerged in the salt solution and the electrical impedance was measured across the BLM using an impedance analyzer (model 4192A, Hewlett Packard, Palo Alto, CA) [25]. The impedance was recorded over a frequency range of $0.01 - 1000$ kHz with a resolution of 50 data points taken with logarithmic spacing. Measurements were taken once at the start of the test before the BLM was pressurized, and once at the end of the test after the BLM had failed. The impedance measurement was used to identify the presence or absence of a BLM on the porous substrate.

2.2.2   Modeling

The pressurization curve of a lipid bilayer can be modeled according to the pressurization of fluid and the flow of fluid through the porous substrate. It has been experimentally determined that after all visible air bubbles have been bled from the lower chamber, approximately 1% of the remaining fluid volume is composed of dissolved air. Therefore it is a basic premise of this model that the change in pressure inside the lower chamber is a result of the contraction and expansion of this volume of air according to Boyle's law, $PV = k$, where P is absolute pressure, V is volume, and k is a constant of proportionality. The constant k can be calculated according to the initial test conditions as

$$k = P_{atm}V_{i,air}, \tag{1}$$

where the initial pressure P_{atm} is one atmosphere, and the initial volume of air $V_{i,air}$ is 1% of the internal volume of the lower test chamber.

It is assumed that at the outset of each trial a BLM covers the substrate pores, effectively

sealing the lower chamber of the test fixture. As the stepper motor pushes the piston forward, it reduces the internal volume of the lower chamber by the amount ΔV_{piston}. This change in volume compresses the air that is dissolved in the aqueous fluid, causing the pressure inside the lower chamber to increase. When the BLM fails, fluid is free to flow out through the porous substrate. For each volume increment of fluid that flows out of the lower chamber, the air within the lower chamber is free to expand by that amount, ΔV_{pores}, thereby decreasing the pressure inside the chamber. This relationship can be summarized as

$$P = \frac{k}{V_{i,air} - \Delta V_{piston} + \Delta V_{pores}}. \tag{2}$$

In these experiments the stepper motor was operated at a fixed frequency, $f_{stepper}$, of 1 Hz, creating a linear piston motion, $\Delta x_{stepper}$, of 1.59 μm per step. Therefore the volume that has been displaced by the motion of the piston can be calculated by

$$\Delta V_{piston} = A_{piston} \Delta x_{stepper} f_{stepper} \Delta t, \tag{3}$$

where A_{piston} is the cross sectional area of the piston and Δt is the amount of time that has elapsed since the start of the experiment.

When the BLM fails, pressure inside of the lower test chamber forces fluid to flow through the porous substrate to the upper chamber of the test fixture, which is open to the atmosphere. The flow rate of fluid exiting the pores can be approximated using Darcy's law for fluid flow through porous media [26],

$$Q = \frac{\kappa A}{\mu L} \Delta P, \tag{4}$$

where Q is the flow rate, κ is the permeability of the medium (which is usually an experimentally determined value), A is the cross sectional area to flow, μ is the viscosity of the fluid, L is the length of flow through the medium, and ΔP is the pressure drop. Flow rate Q can be equivalently written as the time derivative of volume, $Q = \Delta V_{pores}/\Delta t$. For this model, κ will be considered the permeability of the porous substrate and κ' will be considered the combined permeability of the porous substrate and the BLM. The cross sectional area is the area of the substrate that is under pressure, $A_{substrate}$, which is based on the 3.2 mm diameter of the orifice that connects the lower and upper fluid chambers. The pressure drop ΔP is simply the difference between the pressure inside the lower test chamber and the atmosphere, $\Delta P = P - P_{atm}$. Therefore Equation (4) can be rewritten as

$$\Delta V_{pores} = \Delta t \frac{\kappa' A_{substrate}}{\mu L} \left(P - P_{atm} \right). \tag{5}$$

These experiments investigate a BLM that is coated over a substrate with many pores. The BLM is presumed to fail where it covers the pores, and therefore this setup can also be thought of as an array of individual micro-BLMs each covering a pore. In this scenario, all BLMs do not fail at the same pressure, but rather they follow a statistical distribution. It is assumed that the failure pressure of the BLMs follows a normal (Gaussian) distribution. As the pressure in the lower test chamber is increased, BLMs will gradually fail causing a small leak of fluid

through those pores. If only a few BLMs have failed then the leak will be insignificant. When the pressure approaches the mean failure pressure, μ_f, a large number of BLMs will fail at once, causing a larger leak and a measurable drop in pressure.

The combined permeability of the porous substrate and the BLMs changes as the BLMs begin to fail. When all pores are covered by a BLM, the permeability is zero. If all of the BLMs were to fail, then the combined permeability would be that of the porous substrate alone. Between these two cases, it is assumed that the combined permeability varies proportionally with the fraction of BLMs that have failed. However, at the outset of the test a BLM usually does not fully form over every pore. Do to random variability in the formation of the lipid bilayer, some pores remain open. The small fraction of micro-BLMs that do not initially form over a pore, $\chi_{i,f}$, is used as a curve-fitting parameter. The fraction of micro-BLMs that subsequently fail after the start of the test due to pressurization is χ_f. Therefore the overall combined permeability of the porous substrate and the BLM is

$$\kappa' = (\chi_{i,f} + \chi_f) \kappa. \tag{6}$$

χ_f can be equivalently written as

$$\chi_f = (1 - \chi_{i,f}) \Phi(P), \tag{7}$$

where $\Phi(P)$ is the cumulative distribution function of a normal distribution. In this case $\Phi(P)$ represents the fraction of BLMs that fail at a given pressure P, assuming that failure pressure is a random normal variable. $\Phi(P)$ can be computed by integrating the probability density function of a normal distribution [27],

$$\Phi(P) = \frac{1}{\sigma_f \sqrt{2\pi}} \int_{-\infty}^{P} \exp\left(-\frac{(u - \mu_f)^2}{2\sigma_f^2}\right) du, \tag{8}$$

where u is an integration variable.

2.2.3 Results

Figure 16 is a plot of pressure versus piston displacement for the control trials. These traces represent the pressurization of porous substrates without a BLM formed over them. For most pore sizes, no significant pressure buildup was observed, indicating that fluid was free to flow through the porous substrate in the absence of a BLM. For the 0.05 μm pore size, a sizable back-pressure was generated with the stepper motor operating at a frequency of 1 Hz. However, this back-pressure was still small when compared to pressurization of a BLM formed over the same substrate.

The permeability of each porous substrate was determined experimentally. To do this, a porous substrate without a BLM was clamped into the stepper motor test fixture. The stepper motor was turned on at time t_0 and run at a high frequency to generate back-pressure inside the lower chamber. Then the stepper motor was turned off at time t_1 and the back-pressure was allowed to decrease as fluid exited through the pores. The model described in Section 2.2.2 was used to curve-fit the permeability. The model was modified such that ΔV_{piston} was held as a constant value after time t_1 when the piston stopped moving, and the permeability was held
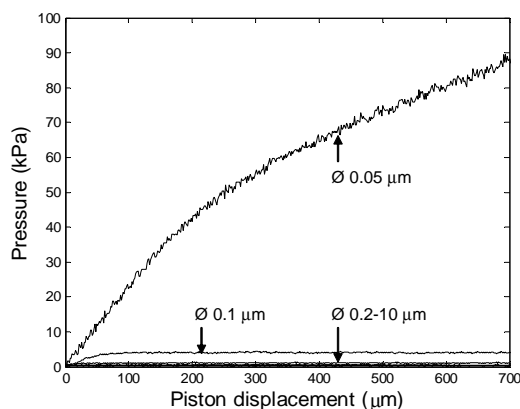
Figure 16: Control trials in which a porous substrate with no BLM was pressurized.

as a constant value for the entire simulation. Figure 17 is an example in which a substrate with 0.2 μm diameter pores was pressurized by running the stepper motor at a frequency of 5 Hz for approximately 35 s. At time $t_1 = 35$ s, the stepper motor was turned off and the back-pressure decreased to zero. Ideally the model should provide a good fit of the experimental pressure curve both when stepper motor is turned on and when it is turned off. However, often times two different permeability values are needed to fit these two different regimes. Before t_1 the modeling of the permeability is complicated by the fact that pressure is increasing due to the piston motion while simultaneously decreasing due to fluid flow through the pores. The model is simplified after t_1 since the piston is stopped. The experimental response in this regime is also cleaner and more repeatable. Therefore a permeability value was chosen that provided the best curve-fit after time t_1, when pressure was decreasing. In the example shown in Figure 17 the permeability was estimated as 8.0×10^{-17} m^2.

Figure $18A$ is a plot of pressure versus piston displacement for ten pressurization trials under the same test conditions of SOPC BLMs formed over substrates with 0.2 μm diameter pores. Figure $18B$ is the same plot for substrates with 2 μm diameter pores. These are typical pressurization curves which have a pressure rise, a peak that represents the bulk failure pressure of the BLM, and a subsequent pressure decrease.

The electrical impedance has been measured for each trial before the BLM was pressurized and again after it failed. For BLMs formed on 0.2 μm pore substrates, Figure $19A$ is a plot of impedance and phase versus frequency for each trial before pressurization, and Figure $19B$ is the same measurement after the BLM failed. Figures $19C$ and $19D$ are the same measurements for 2 μm pore substrates.

The impedance measurements served as a useful way of identifying whether or not a BLM formed over the porous substrate. An electrical impedance measured at the start of the test that reached a maximum of $100 - 1000$ kΩ indicated that a lipid bilayer had fully formed over the porous substrate. The impedance measured after failure occurred was consistently on the order of $1 - 10$ kΩ. This was the same magnitude of resistance of the salt solution alone, implying that the BLM no longer covered the pores of the substrate. Figure 19 supports these trends and
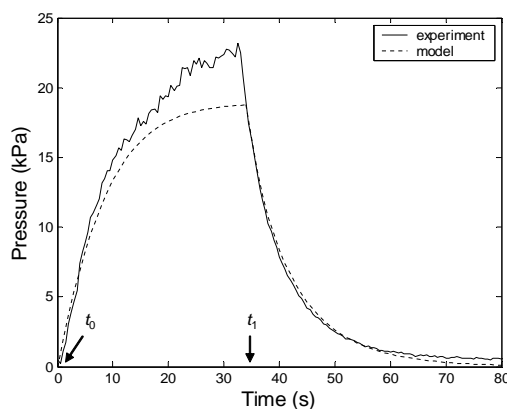
Figure 17: A trial in which a 0.2 μm porous substrate without a BLM was pressurized by running the stepper motor at 5 Hz starting at time t_0, and then turned off at time t_1 to allow pressure to decrease. The experimentally measured curve is marked by a solid line and the model based on a curve-fitted permeability is marked by a dotted line.

shows a clear and repeatable difference between the impedance signatures associated with the presence or absence of a BLM.

Due to the large amount of data collected during this study, every trial is not presented here. Instead, a representative trial from each pore size was chosen and are plotted together in Figures 20A, 20B, and 20C. The data has been separated into three plots so that each can be scaled appropriately. Each plot shows the experimentally measured pressure curve as well as a model pressure curve that was fitted to the data. In each model curve, the mean failure pressure, μ_f, the standard deviation of the failure pressure, σ_f, and the fraction of BLMs that are initially failed, $\chi_{i,f}$, were used as curve-fitting parameters. These parameters are reported in Table 2, as well as the total fraction of failed BLMs at the end of the test, $\chi_{i,f} + \chi_f$, which was determined by the model.

A logarithmic plot of failure pressure versus pore size is shown in Figure 21, where each point represents the mean failure pressure of all trials for that pore size. In this plot data is shown for SOPC and SOPC/CHOL-50 mol%, as measured using the water column test fixture from the previous study and using the stepper motor test fixture from the current study. Data points from the water column test fixture represent the average of six repeated trials while data points from the stepper motor test fixture are the average of ten repeated trials. The experimental results establish a clear trend between the failure pressure of planar BLMs and the pore size of their supporting substrate, demonstrating that failure pressure increases as pore size decreases. On the logarithmic plot from Figure 21 this relationship was nearly linear.

2.2.4 Analysis

The failure pressures measured using the water column test fixture from the previous study were in good agreement with the failure pressures measured using the stepper motor test fixture. The water column test fixture was limited to small pressure measurements, but the step-

23
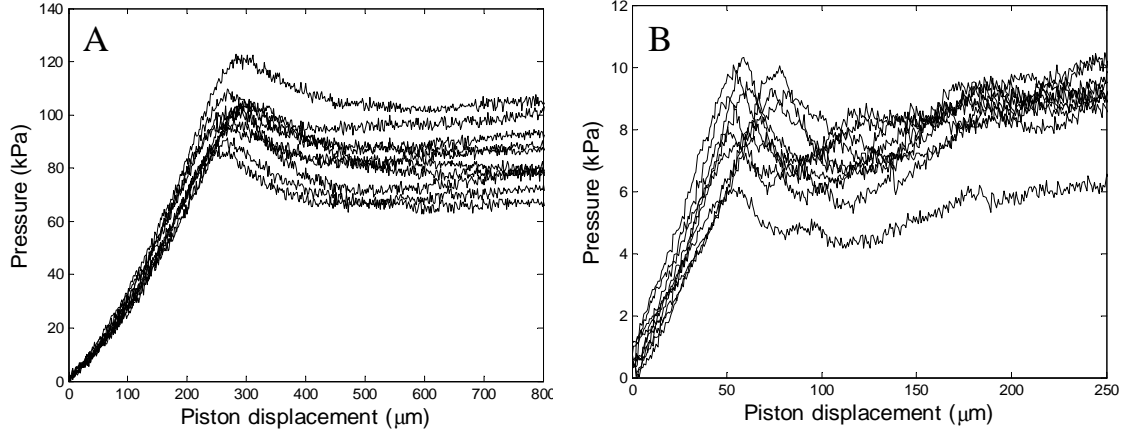
Figure 18: Pressurization curves for ten trials of an SOPC BLM formed on a substrate with (A) 0.2 μm diameter pores, and (B) 2 μm diameter pores.

Table 2: Mean failure pressure, standard deviation, the fraction of BLMs that are initially failed, and the total fraction of failed pores at the end of the test.

Pore Dia. (μm)	μ_f (kPa)	σ_f (kPa)	$\chi_{i,f}$	$\chi_{i,f} + \chi_f$
0.05	405	53	0.180	0.337
0.1	239	3.8	0.027	0.069
0.2	100	0.88	0.015	0.046
0.4	42.0	0.50	0.006	0.051
0.8	22.6	0.38	0.006	0.078
2	9.4	0.13	0.005	0.187
5	3.4	0.068	0.015	0.062
10	1.9	0.054	0.008	0.029
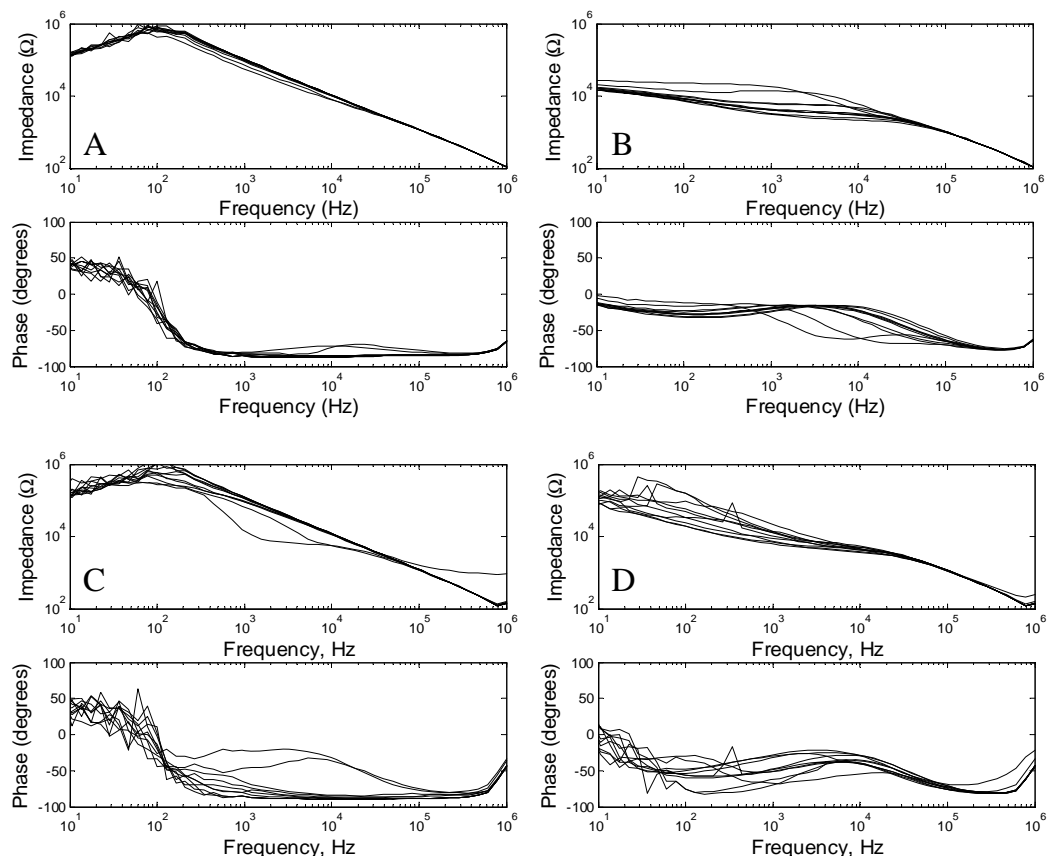
Figure 19: Impedance measurements (*A*) *before* pressurization of an SOPC BLM on a substrate with 0.2 μm diameter pores, (*B*) *after* pressurization of an SOPC BLM on a substrate with 0.2 μm diameter pores, (*C*) *before* pressurization of an SOPC BLM on a substrate with 2 μm diameter pores, and (*D*) *after* pressurization of an SOPC BLM on a substrate with 2 μm diameter pores.
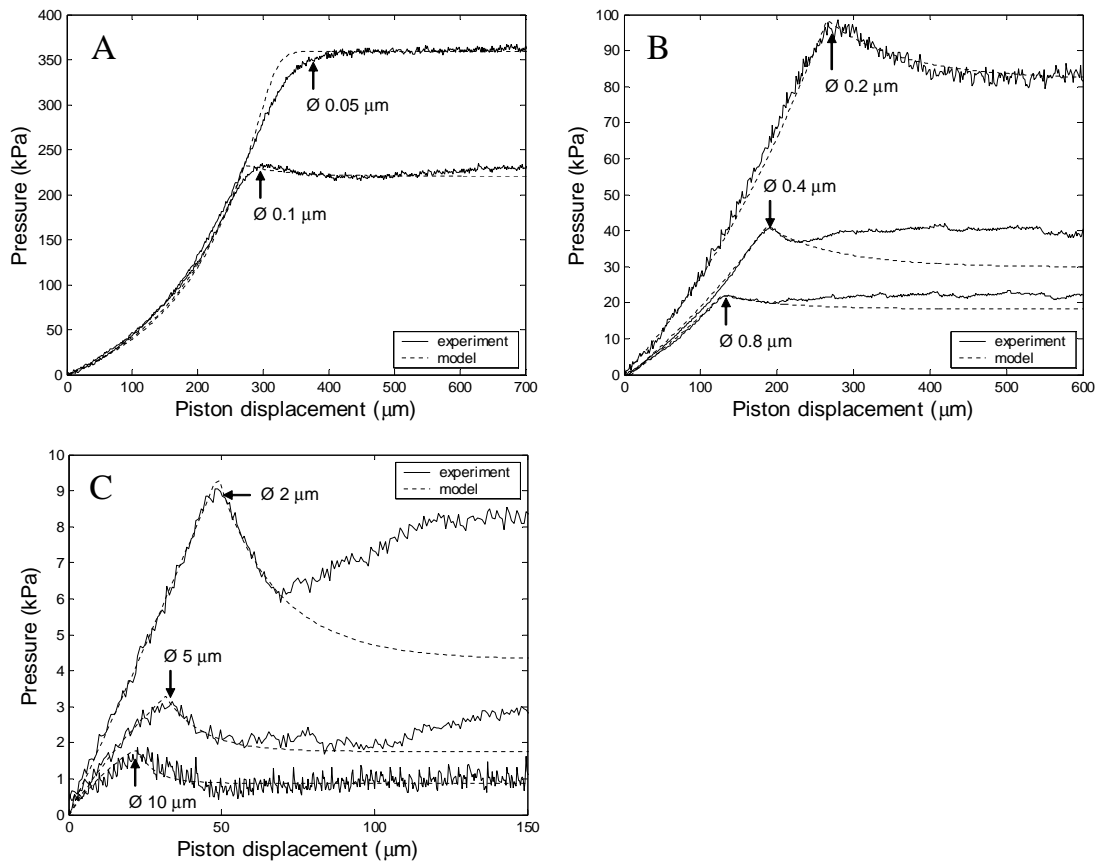
Figure 20: For the pressurization of SOPC, a representative experimental trial from each pore size is marked by a solid line and the predicted response line fitted to each experiment is marked by a dotted line. (*A*) 0.05 μm, and 0.1 μm diameter pores. (*B*) 0.2 μm, 0.4 μm, and 0.8 μm diameter pores. (*C*) 2 μm, 5 μm, and 10 μm diameter pores.

Figure 21: Failure pressure versus pore size. Squares denote SOPC BLMs measured by the stepper motor test fixture; diamonds denote SOPC BLMs measured by the water column test fixture; plus marks denote SOPC/CHOL-50 mol% BLMs measured by the stepper motor test fixture; X marks denote SOPC/CHOL-50 mol% BLMs measured by the water column test fixture.
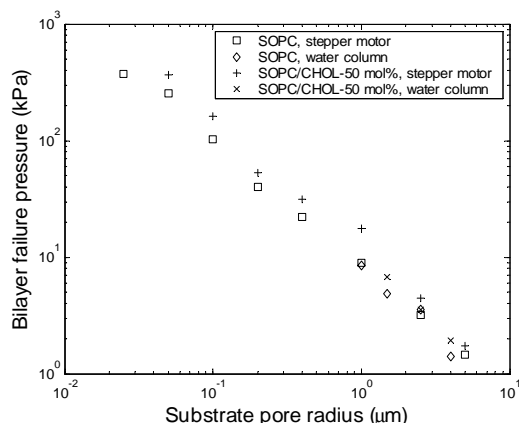
per motor test fixture greatly expanded the range and resolution of pressures and pore sizes that could be tested. The stepper motor test fixture provided an automated application of pressure to the BLM and reduced the amount of interpretation by the operator in determining the failure pressure of the BLM. Figures 18A and 18B show that the pressurization curves generated using the stepper motor test fixture are very repeatable.

Cholesterol is known to increase the strength of saturated and mono-unsaturated BLMs such as SOPC [23, 24]. The experimental results in Figure 21 were consistent with this trend. The failure pressure for a mixture of SOPC and 50 mol% cholesterol was on average 1.5 times greater than that of SOPC alone.

The model presented in Section 2.2.2 and Figure 20 was intended to provide a physical interpretation of the pressurization and failure of the BLMs in this test setup. Most of the parameters that were needed for the model were geometrical or other physical properties of the test fixture and porous substrates. However, the mean failure pressure, standard deviation of failure pressure, and the fraction of initially failed BLMs were left as fitting parameters. Many aspects of the experimental pressure curves were fitted by the model quite well. In most cases, the experimental pressure curve consisted of a pressure rise, a peak, and a steady decay in pressure to some equilibrium value. However, in some instances the pressure did not level off to a constant equilibrium value but rather showed dramatic fluctuations (as seen in Figure 20C for the responses of BLMs formed on substrates with pore diameters of 2 μm and 5 μm). This phenomena could be due to several factors including failed BLMs reforming to block previously open pores, salt from the NaCl solution clogging open pores, and random local pressure fluctuations near the pressure transducer which appear more dramatic for the smaller pressure measurements associated with larger pore sizes. The model can not account for this phenomena because it assumes that the permeability of the substrate is a constant and

that BLMs do not reform after they have failed.

Several interesting insights were gained through the fitting of this model. First, it was found that the bulk failure pressure that was measured in these experiments was close to the curve-fitted mean failure pressure of an individual micro-BLM. In most cases, the curve-fitted mean failure pressure was slightly higher than the bulk failure pressure. However, the two values were close enough that the mean failure pressure can be estimated by simply measuring the bulk failure pressure.

Second, a relationship was determined between the standard deviation of the failure pressure and the shape of the pressurization curve. If the failure of the BLMs has a narrow distribution then most of the micro-BLMs fail together near the mean failure pressure, which is seen as a peak pressure followed by a sharp drop in pressure. This behavior was observed in most trials. However, in some instances the pressure did not reach a local peak, but instead steadily leveled off to the equilibrium pressure. (See, for example, the pressure curve for the 0.05 μm pore size in Figure 20A.) The responses of these BLMs have wider distributions, causing a more gradual pressure rise.

Third, the model provided a way to calculate the fraction of BLMs that have failed at the end of the test, $\chi_{i,f} + \chi_f$, which was reported in Table 2. In these experiments the final equilibrium pressure was nonzero, indicating that some portion of BLMs had not failed. If all BLMs were to fail during the test then the pressure would fall to zero. Instead, the BLMs that do not fail continue to block the substrate pores creating a back pressure in the lower chamber. In all cases the fraction of failed BLMs in Table 2 was less than 0.5, meaning that the test never reaches the true mean failure pressure, μ_f. Also, there was a general trend in which the final fraction of failed BLMs decreased with increasing pore size. This is likely due to the fact that a larger pore allows a greater rate of fluid flux. Therefore with substrates that have large pores, less BLMs are needed to fail to create a measurable pressure drop.

3 Publications

3.1 Papers published in peer-reviewed journals

- Sundaresan, V. B. and Leo, D. J., 2007, Controlled Fluid Transport using ATP-Powered Protein Pumps, Journal of Smart Materials Systems., Vol. 16, No. 2

- Sundaresan, V. B. and Leo, D. J., 2006, Chemo-mechanical Model for actuation based on Biological Membranes, Journal of Intelligent Material Systems and Structures, Vol. 17, 863-870

- Matthews, L., Sundaresan, V. B., Giurgiutiu. V., Leo, D. J., 2006, Bioenergetics and Mechanical Actuation Analysis with Membrane Transport Experiments for Use in Biomimetic Nastic Structures, J. Mater. Res., Vol. 21, No. 8

3.2 Papers published in non-peer-reviewed journals or in conference proceedings

- Sundaresan, V. B. and Leo, D. J., Investigation on High Energy Density Materials Utilizing Biological Transport Mechanisms, Nov 15-21, Proceedings of IMECE-2004, ASME Mechanical Engineering Congress, Anaheim, CA

- Sundaresan, V. B. and Leo, D. J., Chemo-mechanical Model of Biological Membranes for Actuation Mechanisms, Proceedings of SPIE, Volume 5761, Smart Structures and Materials 2005: Active Materials: Behavior and Mechanics pp. 108-118, San Diego, CA

- Sundaresan, V. B. and Leo, D. J., Experimental Investigation for Chemo-Mechanical Actuation using Biological Transport Mechanisms, Proceedings of IMECE-2005, ASME Mechanical Engineering Congress, Nov 5- 11, Orlando, FL.

- Sundaresan, V. B. and Leo, D. J., Protein-based Microhydraulic Transport for Controllable Actuation, Proceedings of SPIE - Volume 6168, Smart Structures and Materials 2006: Electroactive Polymers and Devices, San Diego, CA

- Sundaresan, V. B., Akle, B., Leo, D. J., Investigation on micro-patterned gold-plated polymer substrate for a micro hydraulic actuator, Proceedings of SPIE -Volume 6170, Smart Structures and Materials 2006: Active Materials: Behavior and Mechanics, San Diego, CA.

- Sundaresan, V.B. and Leo, D. J., Microhydraulic Actuation Using Biological Ion Transporters Reconstituted on Artificial BLM, Proceedings of MRS Spring 2006 Meeting, April 15-21, San Francisco, CA.

- Sundaresan, V.B., and Leo, D. J., Actuation using Protein Transporters Driven by Proton Gradients, Proceedings of IMECE-2006, ASME Mechanical Engineering Congress, Nov 5-11, Chicago, Ill.

- Sundaresan, V.B., Leo, D. J., and Goode, B.J., Chemo-electrical Energy Conversion of Adenosine triphosphate in a Biological Ion Transporter, Proceedings of MRS Fall 2006 Meeting, Nov 27-Dec 1, 2006, Hynes Convention Center, Boston, MA

- Sundaresan, V.B., Sarles, S.A., and Leo, D. J., Stack of BioCells Converting ATP to Electrical Power and Possible Applications, Proceedings of MRS Fall 2006 Meeting, Nov 27-Dec 1, 2006, Hynes Convention Center, Boston, MA

- Sundaresan, V.B., Sarles, S.A., and Leo, D. J., Chemo-electrical energy conversion of adenosine triphosphate, March 20, 2007, California Room, Town and Country Resort, San Diego, California.

- Hopkinson, D. P., and Leo, D. J. (2007). Evaluating the mechanical integrity of bilayer lipid membranes using a high precision pressurization system. In Proceedings of SPIE Conference for Smart Structures & Materials/NDE

- Hopkinson, D. P., DeVita, R., and Leo, D. J. (2006). "Evaluating the failure pressure of bilayer lipid membranes by a controllable electromagnetic test fixture. In Proceedings of ASME International Mechanical Engineering Congress and Exposition, IMECE2006-15335.

- DeVita, R., Hopkinson, D., Sundaresan, V. B., and Leo, D. J. (2006). Continuum modeling of bilayer lipid membranes. In Proceedings of MRS

- Hopkinson, D. P., De Vita, R., and Leo, D. J. (2006). Failure pressure of lipid bilayer membranes formed over porous polycarbonate substrates. In Proceedings of SPIE Conference for Smart Structures & Materials/NDE, 6170-70.

3.3 Manuscripts submitted, but not published

- Sundaresan, V. B., Leo, D. J., Homison. C., and Weiland L. M., 2006, Biological Transport Processes for Microhydraulic Actuation, Sensors and Actuators (Chemical: B) (in Press, available on www.sciencedirect.com)

3.4 Technical reports submitted to ARO

- ARO Interim Progress Report 44287MSDRP dated July 31, 2005

4 Report of Inventions

- BioCell to Generate Electrical Power using a Biological Ion Transporter Expending Adenosine Triphosphate

- Biological Transporter Based Actuator for use in Developing Pressure

References

[1] Forterre, Y., Skotheim, J. M., Dumais, J., and Mahadevan, L., "How the Venus flytrap snaps," *Nature*, Vol. 433, January 2005, pp. 421–425.

[2] Darwin, C. and Darwin, F., *The Power of Movement in Plants* , Da Capo Press, New York, 1966.

[3] Hodick, D. and Sievers, A., "On the Mechanism of Trap Closure of Venus flytrap (Dionaea muscipula Ellis)," *Planta*, Vol. 179, June 1989, pp. 32–42.

[4] Delrot, S., Atanassova, R., Gomes, E., and Thevenot, P., "Plasma Membrane Transporters: A Machinery for Uptake of Organic Solutes and Stress Resistance," *Plant Science*, Vol. 161, 2001, pp. 391–404.

[5] Getz, H. and Klein, M., " Characteristics of Sucrose Transport and Sucrose-Induced H^+ Transport on the Tonoplast of Red Beet (Beta vulgaris L.) Storage Tissue," *Plant Physiology*, Vol. 107, No. 2, 1995, pp. 459–467.

[6] dos Santos, A. C., da Silva, W. S., de Meis, L., and Galina, A., "Proton Transport in Maize Tonoplasts Supported by Fructose-1,6-Bisphosphate Cleavage. Pyrophosphate- Dependent Phosphofructokinase as a Pyrophosphate-Regenerating System," *Plant Physiology, American Society of Plant Biologists*, Vol. 133, October 2003, pp. 885–892.

[7] Weise, A., Barker, L., Kuhn, C., Lalonde, S., Buschmann, H., Frommer, W. B., and Ward, J. M., "A New Subfamily of Sucrose Transporters, SUT4, with Low Affinity/High Capacity Localized in Enucleate Sieve Elements of Plants," *Plant Cell*, Vol. 12, August 2000, pp. 1345–1355.

[8] Lalonde, S., Boles, E., Hellmann, H., Barker, L., Patrick, J. W., Frommer, W. B., and Ward, J. M., "The Dual Function of Sugar Carriers: Transport and Sugar Sensing," *Plant Cell*, Vol. 11, 4 1999, pp. 707–726.

[9] Kuhn, C., Barker, L., Burkle, L., and Frommer, W., "Update On Sucrose Transport In Higher Plants," *Journal of Experimental Botany*, Vol. 50, 1999, pp. 935–953.

[10] Burkle, L., Hibberd, J. M., Quick, W. P., Kühn, C., Hirner, B., and Frommer, W. B., "The H^+-Sucrose Cotransporter AtSUT1 Is Essential for Sugar Export from Tobacco Leaves," *Plant Physiology*, Vol. 118(1), 1998, pp. 59–68.

[11] Truernit, E., "Plant physiology: The Importance Of Sucrose Transporters," *Current Biology*, Vol. 11, 2001, pp. R169–R171.

[12] Saccani, J., Castano, S., Desbat, B., and Blaudezy, D., "A Phospholipid Bilayer Supported under a Polymerized Langmuir Film," *Biophysical Journal*, Vol. 85, 2003, pp. 3781–3787.

[13] Sackmann, E., "Supported Membranes: Scientific and Practical Applications," *Science*, Vol. 271, 1996, pp. 43–48.

[14] Sundaresan, V. B., Tan, H., Leo, D. J., and Cuppoletti, J., "Investigation on High Energy Density Materials utilizing Biological Transport Mechanisms," *Proceedings of IMECE-2004, Anaheim, CA, USA*, 2004.

[15] Sundaresan, V. B. and Leo, D. J., "Experimental Investigation for Chemo-mechanical Actuation Using Biological Transport Mechanisms," *Proceedings of IMECE-2005*, American Society of Mechanical Engineers, ASME, Orlando, FL, USA, November 2005.

[16] Sundaresan, V. B. and Leo, D. J., "Protein-based Microhydraulic Transport for Controllable Actuation," *Proceedings of Smart Structures and NDE Conference, San Diego, CA*, SPIE Press, Bellingham, WA, USA, 2006.

[17] Mitchison, J. M. and Swann, M. M., "The mechanical properties of the cell surface I. The cell elastimeter." *Journal of Experimental Biology*, Vol. 31, 1954, pp. 443–460.

[18] Evans, E. and Needham, D., "Physical properties of surfactant bilayer membranes: thermal transitions, elasticity, rigidity, cohesion, and colloidal interactions," *Journal of Physical Chemistry*, Vol. 91, 1987, pp. 4219–4228.

[19] Lim, C. T., Zhou, E. H., and Quek, S. T., "Mechanical models for living cells - a review," *Journal of Biomechanics*, Vol. 39, 2006, pp. 195–216.

[20] Thompson, M., Lennox, R. B., and McClelland, R. A., "Structure and electrochemical properties of microfiltration filter-lipid membrane systems," *Analytical Chemistry*, Vol. 54, No. 1, January 1982, pp. 76–81.

[21] Yoshikawa, K., Hayashi, H., Shimcoka, T., Terada, H., and Ishii, T., "Stable phospholipid membrane supported on porous filter paper," *Biochemical and Biophysical Research Communications*, Vol. 145, No. 3, 1987, pp. 1092–1097.

[22] Hopkinson, D. P., DeVita, R., and Leo, D. J., "Failure pressure of bilayer lipid membranes," *Proceedings of SPIE Conference for Smart Structures & Materials/NDE*, 2006.

[23] Needham, D. and Nunn, R. S., "Elastic deformation and failure of lipid bilayer membranes containing cholesterol," *Biophysical Journal*, Vol. 58, 1990, pp. 997–1009.

[24] Needham, D. and Zhelev, D. V., "The mechanochemistry of lipid vesicles examined by micropipet manipulation techniques," *Vesicles*, edited by M. Rosoff, chap. 9, Marcel Dekker, Inc., New York, NY, USA, 1996, pp. 373–444.

[25] Tien, H. T. and Ottova, A. L., "From self-assembled bilayer lipid membranes (BLMs) to supported BLMs on metal and get substrates to practical applications," *Colloids and Surfaces A*, Vol. 149, 1999, pp. 217–233.

[26] Bear, J., *Dynamics of fluids in porous media*, American Elsevier Publishing Co., Inc., New York, NY, USA, 1972.

[27] Devore, J. L., *Probability and Statistics for Engineering and the Sciences*, Duxbury, Pacific Grove, CA, USA, 5th ed., 2000.